JACS
JOURNAL OF THE AMERICAN CHEMICAL SOCIETY
Article
Cite This: J. Am. Chem. Soc. 2018, 140, 17992−17998
pubs.acs.org/JACS

An Artificial Molecular Shuttle Operates in Lipid Bilayers for Ion Transport

Sujun Chen,[†,‡] Yichuan Wang,[†,‡] Ting Nie,[†] Chunyan Bao,[*,†] Chenxi Wang,[†] Tianyi Xu,[†] Qiuning Lin,[†] Da-Hui Qu,[*,†] Xueqing Gong,[†] Yi Yang,[§] Linyong Zhu,[*,†] and He Tian[†]

[†]Key Laboratory for Advanced Materials and Joint International Research Laboratory of Precision Chemistry and Molecular Engineering, Feringa Nobel Prize Scientist Joint Research Center, School of Chemistry and Molecular Engineering, East China University of Science & Technology, 130 Meilong Road, Shanghai, 200237, China

[§]Optogenetics & Synthetic Biology Interdisciplinary Research Center, State Key Laboratory of Bioreactor Engineering, School of Pharmacy, East China University of Science & Technology, 130 Meilong Road, Shanghai, 200237, China

Supporting Information

ABSTRACT: Inspired by natural biomolecular machines, synthetic molecular-level machines have been proven to perform well-defined mechanical tasks and measurable work. To mimic the function of channel proteins, we herein report the development of a synthetic molecular shuttle, [**2**]**rotaxane 3**, as a unimolecular vehicle that can be inserted into lipid bilayers to perform passive ion transport through its stochastic shuttling motion. The [2]rotaxane molecular shuttle is composed of an amphiphilic molecular thread with three binding stations, which is interlocked in a macrocycle wheel component that tethers a K^+ carrier. The structural characteristics enable the rotaxane to transport ions across the lipid bilayers, similar to a cable car, transporting K^+ with an EC_{50} value of 1.0 μM (3.0 mol % relative to lipid). We expect that this simple molecular machine will provide new opportunities for developing more effective and selective ion transporters.

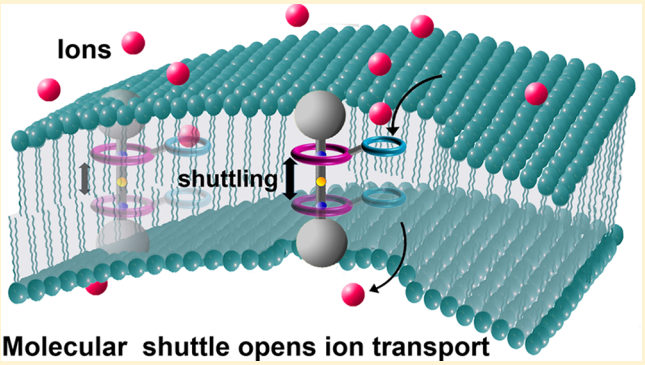

INTRODUCTION

A variety of molecular machines exist in nature. One of the key biological functions of biomolecular machines, such as proteins, is to control substrate transport, which supports life in living organisms.[1,2] In most cases, these transporters have a motor domain that moves along a track to drive the transport of small molecules or ions against a gradient by consuming adenosine triphosphate (ATP) as fuel.[3−5] With an improved understanding of biomolecular machines, scientists have been motivated to develop synthetic molecular machines to perform measurable work by mechanical movements on a molecular level.

Mechanically interlocked molecules, such as rotaxanes and catenanes, have been proven to be promising candidates as synthetic molecular machines.[6−8] In particular, the unique flipping motion between multiple recognition sites in a rotaxane molecular system makes it a highly suitable choice for developing molecular devices. Besides mimicking the functions of ATP-driven protein machines by consuming external energy (light, pH, etc.),[9−11] the stochastic Brownian motion of the wheel along the thread allows the rotaxane to be able to perform work under certain driving forces, such as chemical reactions, gradient concentrations, and so on. One outstanding example of this type of work was mimicking the function of a ribosome,[12] in which an oligopeptide could be synthesized based on the stochastic shuttling of the macrocycle wheel along the thread. Another remarkable application was the passive transport of biologically relevant molecules across membranes, in which different environments changed the host−guest interaction and induced sliding of the wheel along the thread, which enabled the delivery of guest molecules across a nonpolar cell membrane.[13] As is well-known, ion passive transport is also essential for maintaining normal cell function and biological processes. To mimic the functions of channel proteins, specific effort has been devoted to the design and synthesis of artificial systems for passive ion transport across lipid bilayers.[14−17] Although synthetic molecular machines are widely considered to have the potential to facilitate ion transport across membranes through their mechanical motions,[3,8,18] the cases of machines that can perform such tasks have yet to be realized.

Here, we present a study aimed at developing a synthetic [2]rotaxane molecular shuttle that possesses the structural and functional elements necessary to perform ion transport across lipid bilayers. As illustrated in Scheme 1, the designed rotaxane, [**2**]**rotaxane 3**, contains a thread with three positively charged binding stations (**T3**) and a wheel (**CE**) with a

Received: September 14, 2018
Published: November 16, 2018

DOI: 10.1021/jacs.8b09580
J. Am. Chem. Soc. 2018, 140, 17992−17998

Scheme 1. Schematic Representation of the Synthesis and Molecular Structure of [2]Rotaxane 3 and the Proposed Mechanism for K^+ Transport across Lipid Bilayers

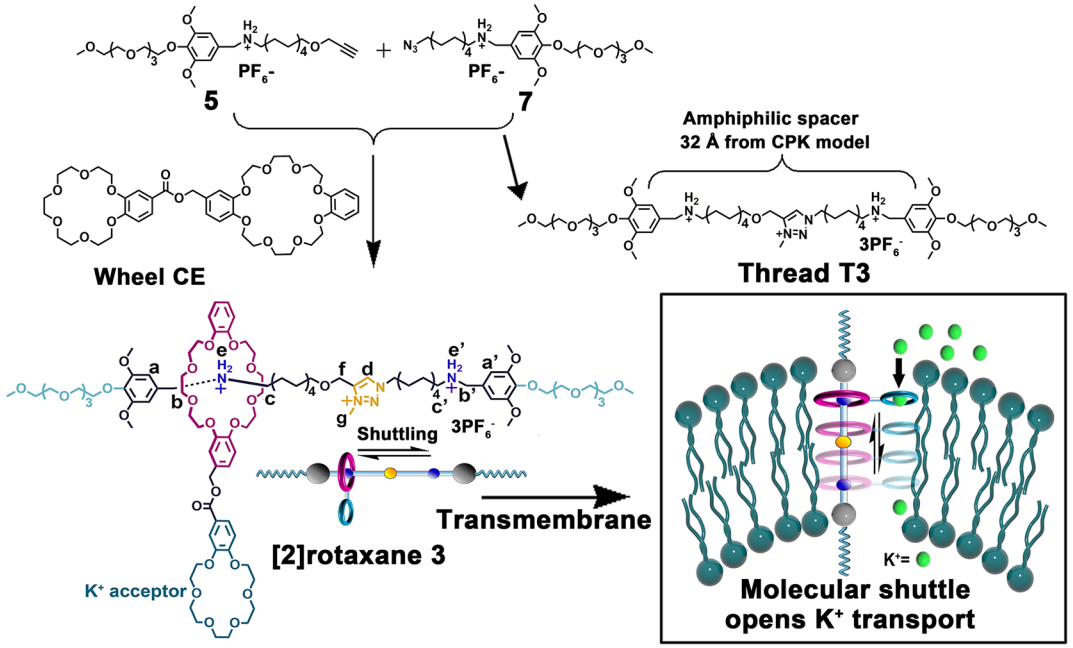

dibenzo-24-crown-8 macrocycle ring component (**DB24C8**) that tethers a K^+ carrier (benzo-18-crown-6, **B18C6**), which is expected to accelerate ion passive transport by the shuttling-based mechanism that begins after the rotaxane inserts into the lipid membrane. To the best of our knowledge, this work represents the first example of a synthetic molecular shuttle tasked with ion transport across lipid bilayers.

RESULTS AND DISCUSSION

Molecular Design and Synthesis. Borrowing the experience of Gokel et al. for designing sophisticated amphiphile-based ion channels,[19] the design principle for such a rotaxane-based transporter should meet the following requirements: (1) the thread component should have an amphiphilic structure and a sufficient molecular length to insert and span the membrane as a cable; (2) an ion receptor should be introduced to the wheel as a car for ion loading and unloading; and (3) the wheel should shuttle among the stations, thus helping the car to transport ions across the membrane. First, based on the channel length of the gramicidin dimer (26−32 Å), an amphiphile with a spacer around 30 Å is considered enough to span the insulator regime of bilayer lipids. Therefore, thread **T3** (as illustrated in Scheme 1) was designed into an amphiphilic structure, in which two tetraethylene glycol groups are introduced at both terminal ends of the thread as the hydrophilic sections and the linker between the two stoppers is used as the amphiphilic spacer (~32 Å estimated from the CPK model). To validate the rationality of the molecular structure of thread **T3**, molecular dynamics (MD) simulation was performed,[20] which exhibited a relatively stable membrane-span structure of **T3** in lipid bilayers (Figure S1). Second, a K^+ receptor, **B18C6**, is tethered to **DB24C8** to enable ion loading and unloading and thus provide the possibility for K^+ passive transport across a lipid bilayer membrane. Third, to achieve wheel shuttling, two benzylalkylammonium hexafluorophosphate (BAA) stations are introduced symmetrically on the thread for stochastic shuttling of the wheel; meanwhile, an *N*-methyltriazolium hexafluorophosphate (MTA) moiety is used as a weaker recognition site for accelerating the shuttling rate of the rotaxane by acting as a central relay.[21] These characteristic features of **[2]rotaxane 3** prompted us to examine the possibility of this molecular shuttle working as a K^+ transporter upon incorporation into a lipid bilayer membrane.

The molecular shuttle **[2]rotaxane 3** was prepared by a threading-followed-stoppering strategy, and all of the compounds were verified by ^{1}H and ^{13}C NMR spectroscopies and HR-ESI spectrometry (Schemes S1−S4). To verify the interlocked structure of the rotaxane, partial ^{1}H NMR spectra of **[2]rotaxane 3**, thread **T3**, and wheel **CE** in d_6-DMSO were investigated.

As shown in Figure 1, compared with thread **T3**, the ^{1}H NMR spectrum of **[2]rotaxane 3** showed two sets of peaks at 6.65 and 7.15 ppm for the aromatic protons Ha and Ha′, respectively, which could be clearly assigned as complexed and uncomplexed thread protons. The two peaks indicated that the

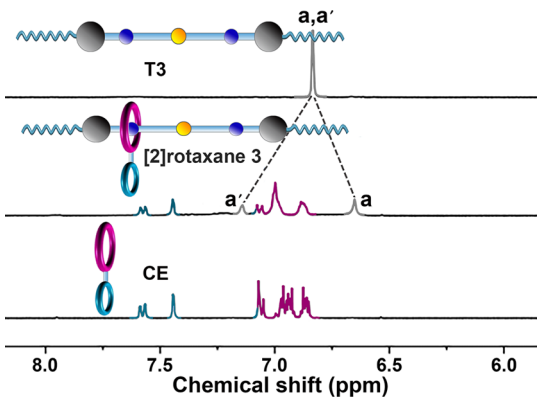

Figure 1. Partial ^{1}H NMR spectra (400 MHz) of thread **T3**, **[2]rotaxane 3**, and wheel **CE**. The concentrations are 1.0×10^{-3} M in d_6-DMSO at 298 K.

DOI: 10.1021/jacs.8b09580
J. Am. Chem. Soc. 2018, 140, 17992−17998

wheel stayed at one of the ammonium stations on the NMR time scale and that the sliding rate of the wheel on the thread component was relatively slow. To explore the rate of the wheel shuttling, NMR exchange spectroscopy (2D-EXSY) analysis was performed on [2]**rotaxane 3**, in which $CDCl_3$/CD_3CN (v/v, 1:1) was used as the solvent. After data processing, the shuttling rate k was calculated to be 0.082 Hz (Table 1, Figures S2−5 and Table S1).[22] As known, the shuttling rate of rotaxane is greatly affected by microenvironments (solvents, temperature, etc.);[23] this value does not represent the actual shuttling rate of [2]**rotaxane 3** in the lipid bilayers. However, the existing shuttling motion sliding along such a long thread component provides the possibility to help the ionophore **B18C6** on the rotaxane wheel to transport ions across lipid bilayers.

Table 1. Physical Properties and Quantitative Analysis of the Transmembrane Activity of Transporters in the LUVs⊃HPTS Assay

transporter	EC_{50}[a]	Clogp[b]	k (Hz)[c]
[2]**rotaxane 3**	1.0 (3.0)	7.22	0.082
T3	26.9 (81.0)	7.03	
CE	N.D.	1.89	
B18C6	N.D.	0.78	
[2]**rotaxane 2**	6.7 (20.0)	8.02	N.D.
T2	18.0 (54.0)	7.77	
[2]**rotaxane 1**	N.D.	8.72	

[a]EC_{50} defined as the final concentration, μM (mol % relative to lipid), of transporter required to obtain 50% activity at t = 300 s. [b]Calculated logp using ALOGPS 2.1, an estimate of lipophilicity where p is the partition coefficient between octanol and water. [c]Estimated shuttling rate determined by 2D-EXSY NMR analysis in $CDCl_3$/CD_3CN. N.D. means not determined.

Ion Transport Activity and Mechanism Study. To explore the ability for ion transmembrane transport of [2]**rotaxane 3**, a well-established fluorescence assay with large, unilamellar lipid vesicles entrapping a pH-sensitive fluorescent probe, 8-hydroxypyrene-1,3,6-trisulfonic acid (LUVs⊃HPTS), was carried out.[17c,19,24,25] The experimental process is described as follows (Figure S6): in a LUVs⊃HPTS vesicles buffer, a pH gradient was applied by addition of KOH (i.e., ΔpH = 0.8) in the extravesicular buffer; then the addition of transporters induced the pH gradient collapse via a H^+ efflux or OH^- influx, which led to the change in the ratio of fluorescence intensity at 510 nm (I_{450}/I_{405}) of HPTS entrapped inside the vesicles. For comparison, the corresponding two subunits, thread **T3** and wheel **CE**, were also characterized in the same conditions. After data processing (Figure S7), Figure 2A shows the concentration-dependent ion transport activity of [2]**rotaxane 3** and reveals an EC_{50} (the effective concentration required for 50% activity) value of 1.0 μM (3.0 mol %, relative to lipid, as listed in Table 1). After comparison, [2]**rotaxane 3** exhibits significantly greater transport ability than that of subunits **T3** and **CE** (Figure S8−11). Although **T3** showed some activity, the increase in its EC_{50} to 26.9 μM (81.0 mol %), which was nearly 27-fold higher than that of [2]**rotaxane 3**, implied that the rotaxane structure is a critical factor that affects the transport efficiency. Further plotting the observed rate constant k_{obs} against the concentrations (Figure 2B), the linear correlation indicated the unimolecular active structure of [2]**rotaxane 3** for ion transport.

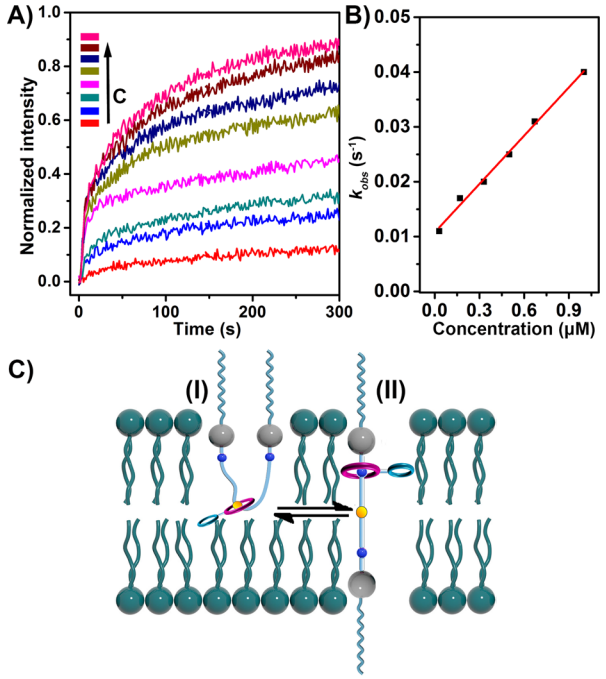

Figure 2. (A) Representative concentration-dependent enhancement of the ion transport activity of [2]**rotaxane 3** at 0.03−13.32 μM (0.1−40.0 mol %, relative to lipid). (B) Plot of pseudo-first-order rate constants (k_{obs}) versus μM of [2]**rotaxane 3** at low concentrations. (C) Proposed insertion mode of rotaxane in lipid bilayers.

A LUV fluorescence assay with 5(6)-carboxyfluorescein (CF) dye encapsulated in liposomes at its self-quenching concentration was carried out to test membrane stability during the ion transport process (Figure S12). The percentage of CF leakage was determined by monitoring the fluorescence intensity of released CF and compared to a 100% release by destroying the liposomes using Triton-X. Addition of [2]-**rotaxane 3** (1.67 μM) and thread **T3** (6.67 μM) led to a low CF leakage (<10%); however, melittin (a membrane lysing agent)[26] at 10 nM resulted in efflux of 85% CF dye from LUVs. It indicated that [2]**rotaxane 3** does not significantly alter the integrity of the membrane, and the role of guest-induced membrane destabilization by forming transient pores was relatively small. Of course, the nonselective membrane disruption for ion transport should not be completely ruled out since the CF leakage was not strictly absent. A preincorporated LUVs⊃HPTS assay was further performed, in which [2]-**rotaxane 3** was already mixed with the phospholipid. The comparable transport activity (4 mol %, Figure S13) confirmed that the ion transport of the rotaxane mainly functions by inserting into the lipid membrane. Therefore, based on the amphiphilic and unimolecular active structure of [2]**rotaxane 3**, the logically possible insertion mode can be assumed as illustrated in Figure 2C. One is the U-shaped insertion state (I), and the other is the transmembrane state (II), in which I can also convert to II by the penetration of one of the head groups.[27]

To find out which one was predominant for ion transport of [2]**rotaxane 3**, a voltage clamp measurement was further performed across the planar bilayer membrane using KCl as an electrolyte.[28] As illustrated in Figure 3, the addition of

DOI: 10.1021/jacs.8b09580
J. Am. Chem. Soc. 2018, 140, 17992−17998

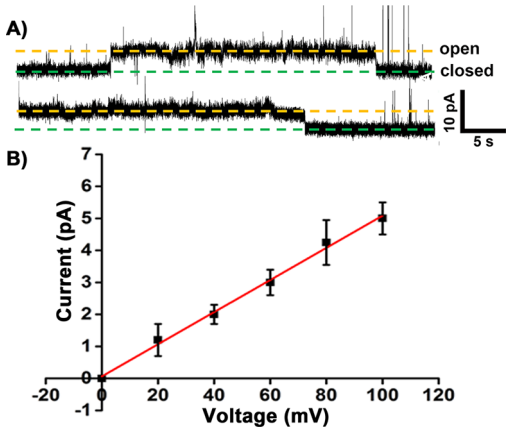

Figure 3. (A) Current recordings of [2]**rotaxane 3** (2.5 μM) from a single channel at 100 mV holding potential in a symmetrical 1 M KCl solution. (B) Linear $I-V$ plots of [2]**rotaxane 3** with varied holding potentials.

[2]**rotaxane 3** produced regular square-like signals with considerably long opening times (Figure 3A, Figure S14) and ohmic $I-V$ profiles (Figure 3B), which indicated the formation of a stable channel or pore across the bilayer membrane. Considering the matching length of rotaxane with the thickness of the insulator regime of lipid bilayers, it can be concluded that ion transport of [2]**rotaxane 3** occurs mostly from the unimolecular transmembrane insertion (II) in the lipid bilayer instead of from the transient distribution of molecules in the membrane.

To explore the action of **B18C6** on the ion transport of [2]**rotaxane 3**, both cation and anion selectivity were recorded. As illustrated in Figure 4A, the variation of cations exhibited different transport activity and followed the order $K^+ > Rb^+ \geq Cs^+ > Na^+ > Li^+$. This order was consistent with the Eisenman sequence IV,[29] which suggested that the ion selectivity of [2]**rotaxane 3** does not correspond to the energetic penalty for ion dehydration and is more related to the ion recognition of **B18C6**. In contrast, **T3** without a K^+ recognition receptor provided little difference in ion transport activity toward various cations (Figure S15). On further variation of anions by changing A^- (where $A^- = F^-$, Cl^-, Br^-, and I^-) in an extravesicular buffer, the transport activity of [2]**rotaxane 3** exhibited an insignificant difference (Figure 4B, Figure S16). A Cl^--sensitive Lucigenin vesicle assay (Figure 4C, Figure S17) was further performed, and the negligible activity of [2]**rotaxane 3** indicated that Cl^- transport was limited by the rotaxane-based transporter. It can be concluded that the presence of **B18C6** enabled K^+ selectivity in [2]**rotaxane 3**, and thus either a K^+/OH^- symport or K^+/H^+ antiport process was responsible for the balance of pH variation inside and outside of the vesicles in the LUVs⊃HPTS assay. To further explore which process is predominant, the transport activity of [2]**rotaxane 3** in the absence and presence of valinomycin, a selective K^+ transporter, was also investigated. As illustrated in Figure 4D (Figure S18), the addition of valinomycin caused the fluorescence intensity to increase by 30%. In contrast, the same amount of valinomycin itself resulted in only a 5% increase in the fluorescence intensity. These results support that the rotaxane can also transport OH^- and K^+/OH^- symport to balance the charges inside and outside of the LUVs.[30] Based on the importance for selectively transporting K^+, Na^+, and Cl^- in biological systems,

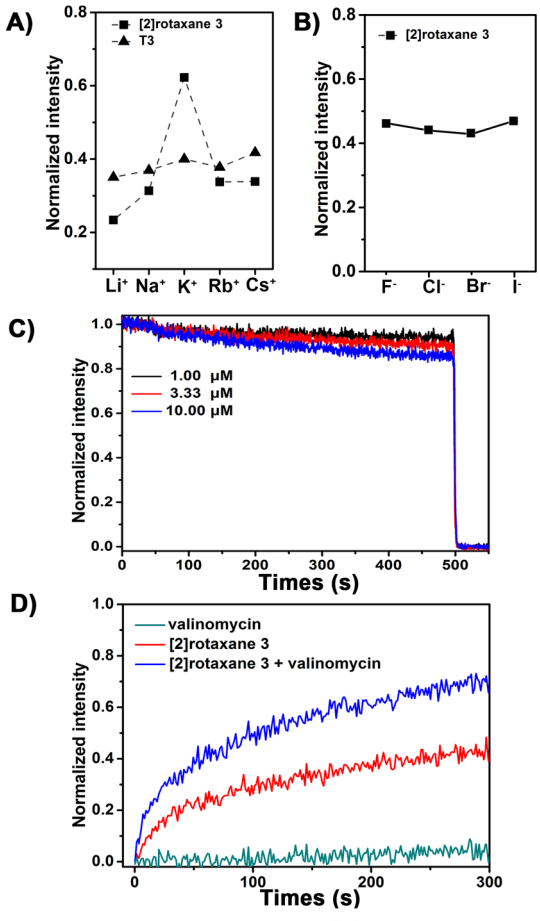

Figure 4. (A) Cation selectivity assay for [2]**rotaxane 3** (3.33 μM) and **T3** (13.67 μM). (B) Anion selectivity assay for [2]**rotaxane 3** (0.67 μM). (C) Lucigenin assay by [2]**rotaxane 3** at different concentrations. (D) HPTS fluorescence assay for [2]**rotaxane 3** (0.67 μM) with or without valinomycin (5 pM).

we further performed a patch-clamp assay to quantitatively compare the permeability ratios of these ions by determining reversal potentials (Figures S19 and S20). Calculations based on the Goldman–Hodgkin–Katz (GHK) flux equation[31] revealed a K^+/Cl^- permeability ratio (P_{K^+}/P_{Cl^-}) of 28 and Na^+/K^+ permeability ratio (P_{Na^+}/P_{K^+}) of 0.2. The high selectivity between and K^+ and Cl^- was in agreement with the Lucigenin vesicle assay that showed the Cl^- transport was not effective. Therefore, the excellent K^+ selectivity indicated that the ion transport of [2]**rotaxane 3** should result from the ion loading and release of **B18C6**.

Finally, the effect of the shuttling motion on the transport activity of [2]**rotaxane 3** was explored. As shown in Figure 5A, two additional rotaxanes, [2]**rotaxane 2** (Scheme S4) and [2]**rotaxane 1** (Scheme S5), bearing two and one of the recognition site(s), respectively, were designed and synthesized as reference compounds for comparison. The energy profiles indicate that three rotaxanes had different thermodynamic profiles and performed the shuttling motion at different rates (Figure 5B). [2]**rotaxane 3** bears three cationic stations in which wheel CE should be thermodynamically trapped in the ammonium energy well due to their relatively stronger interaction, and thus the symmetric existence induced the stochastic shuttling between the two ammonium (BAA) stations. The introduction of a weak recognition site of

DOI: 10.1021/jacs.8b09580
J. Am. Chem. Soc. 2018, 140, 17992–17998

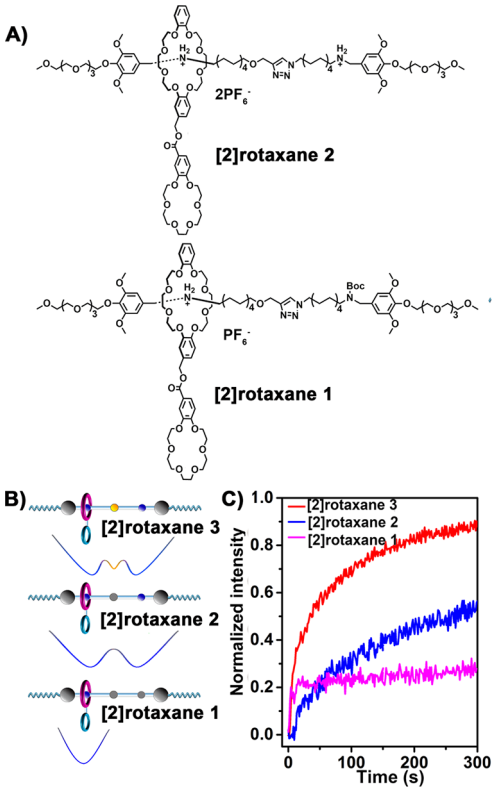

Figure 5. (A) Molecular structures of [2]**rotaxane 2** and [2]**rotaxane 1**. (B) Energy profiles representing the free energy of the rotaxanes during the wheel's movement along the thread axle. (C) Comparison of transport activity of the rotaxanes at 10 μM.

MTA in the middle of the thread would decrease the shuttling energy barrier and, thus, speed up the shuttling rate. Compared with [2]**rotaxane 3**, [2]**rotaxane 2**, with two symmetrical BAA stations, should have a slower shuttling rate. The shuttling rate of [2]**rotaxane 2** was also estimated by 2D-EXSY experiments (Figures S21), from which no obvious cross-peaks were observed even at τ_m = 500 ms. Although the shuttling rate failed to be calculated, the shuttling motion of [2]**rotaxane 2** undoubtedly exists by Brownian motion between the two recognition sites.[32] For [2]**rotaxane 1**, the unique BAA station made the wheel primarily circle at the ammonium site, causing difficulty in shuttling the wheel on the thread component. The transport activities of [2]**rotaxane 2** and [2]**rotaxane 1** were also explored by the LUVs⊃HPTS assay (Figure 5C, Figures S22–S24). As expected, both of the reference rotaxanes exhibited much lower transmembrane activity than that of [2]**rotaxane 3**, especially for [2]**rotaxane 1**. The results are also summarized in Table 1, which reveals the EC_{50} value of [2]**rotaxane 2** is 6.7 μM (20.0 mol % relative to lipid), and the EC_{50} value of [2]**rotaxane 1** is not determined. Considering their similar molecular properties (Clogp listed in Table 1), the variable transport activities of the three rotaxanes were probably deduced by the differences in the charge numbers or the shuttling motion rate. The charge effect on transport activity was investigated between threads **T2** and **T3**, which exhibited the opposite relationship of activity-charge numbers, and the transport activity of **T2** with two positive charges was even higher than **T3** with three charges (Figures S25 and S26). Therefore, it indicated that the shuttling motion might play a key role in improving ion transport in the rotaxanes.

Effect of pH-Regulated Shuttling on Transport Activity. If the above shuttling-based mechanism works, the operation on the shuttling rate would affect the transport activity of rotaxanes. As known, the ammonium sites on the thread of [2]**rotaxane 3** were pH-sensitive groups and can be deprotonated by addition of base, which was always applied to control the shuttling movement in rotaxane systems (as illustrated in Figure 6A). Therefore, pH variation was used to

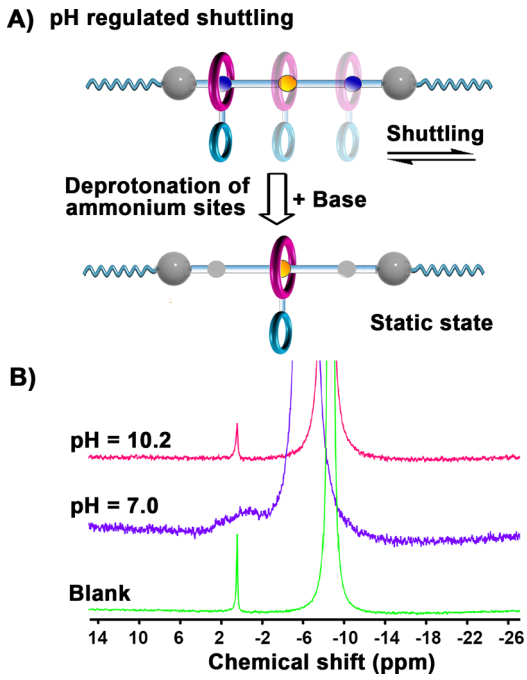

Figure 6. (A) Schematic presentation of pH-regulated shuttling of [2]**rotaxane 3**. (B) ^{23}Na NMR spectra of [2]**rotaxane 3** (0.13 mM) at different pH values, in which the LUVs were prepared with [Na^+ in] = 200 mM, [Na^+ out] ≈ 200 mM, and [$DyCl_3$ out] = 4.85 mM.

control the shuttling motion of [2]**rotaxane 3**. The ^{1}H NMR spectra of [2]**rotaxane 3** demonstrated that the shuttling motion of the wheel between the two BAA stations can be halted in response to the addition of a base and that the wheel moves to the MTA station in a static state due to deprotonation of the ammonium moieties (Figure S27). This result indicates that [2]**rotaxane 3** can reversibly switch between a dynamic shuttling state and a static state in response to pH stimuli. To evaluate the ion transport of [2]**rotaxane 3** with different shuttling motions by pH control, a variable-pH ^{23}Na NMR vesicle assay was carried out as shown in Figure 6B.[33] The ^{23}Na NMR method relies on a shift reagent composed of sodium tris(polyphosphate) and dysprosium chloride hexahydrate, which results in two ^{23}Na NMR peaks when added to a LUVs solution: an intravesicular one that is not affected and an extravesicular one that shifts upfield. At pH = 7.0, the resonance signals for Na^+ both inside and outside of the vesicles broadened with the addition of [2]**rotaxane 3**, suggesting that fast Na^+ exchange was initiated by the dynamic rotaxane system. However, under basic conditions (pH = 10.2), the addition of rotaxane resulted in narrow Na^+ signals, which were similar to those of the blank (Table S2), indicating that the static rotaxane did not efficiently activate Na^+ exchange. All these results indicate that the increased pH deprotonates the ammonium stations and locates the wheel

DOI: 10.1021/jacs.8b09580
J. Am. Chem. Soc. 2018, 140, 17992–17998

statically at the MTA station; thus the prevented shuttling of the wheel blocks the ion exchange across the lipid layers. The pH control experiment is in good agreement with our shuttling-based transport mechanism, and the whole process can be proposed as illustrated in Scheme 1, which shows that the rotaxane inserts into the membrane, similar to a cable, and that the shuttling motion helps the wheel car passively ferry ions across the lipid bilayers.

CONCLUSION

In conclusion, we have demonstrated that a rotaxane-based molecular shuttle, [2]**rotaxane 3**, can function as a vehicle for ion transport across lipid bilayers. Transport experiments show that the rotaxane can display K^+ selectivity due to **B18C6** recognition preference and exhibit unimolecular transport activity with EC_{50} at 1.0 μM (3.0 mol % relative to lipid). The relationship between the molecular structure and transport performance supported the shuttling-based mechanism of [2]**rotaxane 3** for ion transport across the lipid membrane. Through rational molecular design, we herein expect to provide a new method for designing ion transport systems and for extending applications of these fascinating rotaxanes. Work along this line of inquiry is currently underway in our laboratory.

ASSOCIATED CONTENT

Supporting Information

The Supporting Information is available free of charge on the ACS Publications website at DOI: 10.1021/jacs.8b09580.

Synthesis and characterization of compounds, supplementary HPTS data, and general procedures; appendix of NMR and mass spectra of new compounds (PDF)

AUTHOR INFORMATION

Corresponding Authors

*baochunyan@ecust.edu.cn
*dahui_qu@ecust.edu.cn
*linyongzhu@ecust.edu.cn

ORCID

Da-Hui Qu: 0000-0002-2039-3564
Xueqing Gong: 0000-0002-9566-7427
Linyong Zhu: 0000-0002-0398-7213
He Tian: 0000-0003-3547-7485

Author Contributions

‡S. Chen and Y. Wang contributed equally.

Notes

The authors declare no competing financial interest.

ACKNOWLEDGMENTS

This work was supported by NSFC/China (21472044, 21425311, 21790361, 21421004), Shanghai Municipal Science and Technology Major Project (Grant No. 2018SHZDZX03), the Fundamental Research Funds for the Central Universities (222201717003), and the Program of Introducing Talents of Discipline to Universities (B16017).

REFERENCES

(1) Finnigan, G. C.; Hanson-Smith, V.; Stevens, T. H.; Thornton, J. W. Evolution of increased complexity in a molecular machine. *Nature* **2012**, *481*, 360−364.

(2) (a) Schliwa, M.; Woehlke, G. *Nature* **2003**, *422*, 759−765. (b) Piccolino, M. Biological machines: from mills to molecules. *Nat. Rev. Mol. Cell Biol.* **2000**, *1*, 149−152.

(3) Watson, M. A.; Cockroft, S. L. Man-made molecular machines: membrane bound. *Chem. Soc. Rev.* **2016**, *45*, 6118−6129.

(4) Zhao, X.; Zhang, K.; Boquoi, T.; Hu, B.; Motaleb, M. A.; Miller, K. A.; James, M. E.; Charon, N. W.; Manson, M. D.; Norris, S. J.; Li, C.; Liu, J. Cryoelectron tomography reveals the sequential assembly of bacterial flagella in Borrelia burgdorferi. *Proc. Natl. Acad. Sci. U. S. A.* **2013**, *110*, 14390−14395.

(5) Arai, S.; Saijo, S.; Suzuki, K.; Mizutani, K.; Kakinuma, Y.; Ishizuka-Katsura, Y.; Ohsawa, N.; Terada, T.; Shirouzu, M.; Yokoyama, S.; Iwata, S.; Yamato, I.; Murata, T. Rotation mechanism of Enterococcus hirae V_1-ATPase based on asymmetric crystal structures. *Nature* **2013**, *493*, 703−707.

(6) (a) Kassem, S.; Leeuwen, T.; Lubbe, A. S.; Wilson, M. R.; Feringa, B. L.; Leigh, D. A. Artificial molecular motors. *Chem. Soc. Rev.* **2017**, *46*, 2592−2621. (b) Eelkema, R.; Pollard, M. M.; Vicario, J.; Katsonis, N.; Ramon, B. S.; Bastiaansen, C. W.M.; Broer, D. J.; Feringa, B. L. Molecular machines: nanomotor rotates microscale objects. *Nature* **2006**, *440*, 163−163.

(7) (a) Sauvage, J. P. From chemical topology to molecular machines (Nobel lecture). *Angew. Chem., Int. Ed.* **2017**, *56*, 11080−11093. (b) Ragazzon, G.; Baroncini, M.; Silvi, S.; Venturi, M.; Credi, A. Light-powered autonomous and directional molecular motion of a dissipative self-assembling system. *Nat. Nanotechnol.* **2015**, *10*, 70−75.

(8) (a) Pezzato, C.; Cheng, C. Y.; Stoddart, J. F.; Astumian, R. D. Mastering the nonequilibrium assembly and operation of molecular machines. *Chem. Soc. Rev.* **2017**, *46*, 5491−5507. (b) Cheng, C.; McGonigal, P. R.; Schneebeli, S. T.; Li, H.; Vermeulen, N. A.; Ke, C.; Stoddart, J. F. An artificial molecular pump. *Nat. Nanotechnol.* **2015**, *10*, 547−553.

(9) (a) Erbas-Cakmak, S.; Fielden, S. D.; Karaca, U.; Leigh, D. A.; McTernan, C. T.; Tetlow, D. J.; Wilson, M. R. Rotary and linear molecular motors driven by pulses of a chemical fuel. *Science* **2017**, *358*, 340−343. (b) Kassem, S.; Lee, A. T.L.; Leigh, D. A.; Markevicius, A.; Solà, J. Pick-up, transport and release of a molecular cargo using a small-molecule robotic arm. *Nat. Chem.* **2016**, *8*, 138−143. (c) Kay, E. R.; Leigh, D. A.; Zerbetto, F. Synthetic molecular motors and mechanical machines. *Angew. Chem., Int. Ed.* **2007**, *46*, 72−191.

(10) (a) Qu, D.-H.; Wang, Q.-C.; Zhang, Q.-W.; Ma, X.; Tian, H. Photoresponsive host−guest functional systems. *Chem. Rev.* **2015**, *115*, 7543−7588. (b) Tian, H.; Wang, Q.-C. Recent progress on switchable rotaxanes. *Chem. Soc. Rev.* **2006**, *35*, 361−374. (c) Li, S. H.; Zhang, H.-Y.; Xu, X. F.; Liu, Y. Mechanically selflocked chiral gemini-catenanes. *Nat. Commun.* **2015**, *6*, 7590.

(11) Yang Xue, M.; Yang, Y.; Chi, X. D.; Yan, X. Z.; Huang, F. H. Development of pseudorotaxanes and rotaxanes: from synthesis to stimuli-responsive motions to applications. *Chem. Rev.* **2015**, *115*, 7398−7501.

(12) Lewandowski, B.; De Bo, G.; Ward, J. W.; Papmeyer, M.; Kuschel, S.; Aldegunde, M. J.; Gramlich, P. M.E.; Heckmann, D.; Goldup, S. M.; D'Souza, D. M.; Fernandes, A. E.; Leigh, D. A. Sequence-specific peptide synthesis by an artificial small-molecule machine. *Science* **2013**, *339*, 189−193.

(13) Bao, X.; Isaacsohn, I.; Drew, A. F.; Smithrud, D. B. Determining the Intracellular Transport Mechanism of a Cleft−[2] Rotaxane. *J. Am. Chem. Soc.* **2006**, *128*, 12229−12238.

(14) (a) Hille, B. *Ion Channels of Excitable Membranes*, 3rd ed.; Sinauer Associates: Sunderland, MA, 2001. (b) Matile, S.; Fyles, T. Transport across membranes. *Acc. Chem. Res.* **2013**, *46*, 2741−2742.

(15) (a) Gale, P. A.; Davis, J. T.; Quesada, R. Anion transport and supramolecular medicinal chemistry. *Chem. Soc. Rev.* **2017**, *46*, 2497−2519. (b) Gokel, G. W.; Mukhopadhyay, A. Synthetic models of cation-conducting channels. *Chem. Soc. Rev.* **2001**, *30*, 274−286. (c) Kim, D. S.; Sessler, J. L. Calix [4] pyrroles: versatile molecular containers with ion transport, recognition, and molecular switching functions. *Chem. Soc. Rev.* **2015**, *44*, 532−546.

DOI: 10.1021/jacs.8b09580
J. Am. Chem. Soc. 2018, 140, 17992−17998

(16) (a) Busschaert, N.; Park, S. H.; Baek, K. H.; Choi, Y. P.; Park, J.; Howe, E. N.W.; Hiscock, J. R.; Karagiannidis, L. E.; Marques, I.; Felix, V.; Namkung, W.; Sessler, J. L.; Gale, P. A.; Shin, I. A synthetic ion transporter that disrupts autophagy and induces apoptosis by perturbing cellular chloride concentrations. *Nat. Chem.* **2017**, *9*, 667−675. (b) Saha, T.; Gautam, A.; Mukherjee, A.; Lahiri, M.; Talukdar, P. Chloride Transport through Supramolecular Barrel-Rosette Ion Channels: Lipophilic Control and Apoptosis-Inducing Activity. *J. Am. Chem. Soc.* **2016**, *138*, 16443−16451. (c) Li, H.; Valkenier, H.; Judd, L. W.; Brotherhood, P. R.; Hussain, S.; Cooper, J. A.; Jurcek, O.; Sparkes, H. A.; Sheppard, D. N.; Davis, A. P. Efficient, non-toxic anion transport by synthetic carriers in cells and epithelia. *Nat. Chem.* **2016**, *8*, 24−32. (d) Schneider, S.; Licsandru, E.-D.; Kocsis, I.; Gilles, A.; Dumitru, F.; Moulin, E.; Tan, J.; Lehn, J.-M.; Giuseppone, N.; Barboiu, M. Columnar self-assemblies of triarylamines as scaffolds for artificial biomimetic channels for ion and for water transport. *J. Am. Chem. Soc.* **2017**, *139*, 3721−3727.

(17) (a) Su, G.; Zhang, M.; Si, W.; Li, Z. T.; Hou, J. L. Directional potassium transport through a unimolecular peptide channel. *Angew. Chem., Int. Ed.* **2016**, *55*, 14678−14682. (b) Lang, C.; Li, W.; Dong, Z.; Zhang, X.; Yang, F.; Yang, B.; Deng, X.; Zhang, C.; Xu, J.; Liu, J. Biomimetic transmembrane channels with high stability and transporting efficiency from helically folded macromolecules. *Angew. Chem., Int. Ed.* **2016**, *55*, 9723−9727. (c) Ren, C.; Shen, J.; Zeng, H. Combinatorial Evolution of Fast-Conducting Highly Selective K +-Channels via Modularly Tunable Directional Assembly of Crown Ethers. *J. Am. Chem. Soc.* **2017**, *139*, 12338−12341.

(18) (a) Chhun, C.; Richard-Daniel, J.; Kempf, J.; Schmitzer, A. R. Transport of macrocyclic compounds across phospholipid bilayers by umbrella-rotaxanes. *Org. Biomol. Chem.* **2013**, *11*, 6023−6028. (b) Baroncini, M. L.; Vet, C.; Groppi, J.; Silvi, S.; Credi, A. Making and operating molecular machines: a multidisciplinary challenge. *ChemistryOpen* **2018**, *7*, 169−179.

(19) Wang, W.; Li, R.; Gokel, G. W. Membrane-Length Amphiphiles Exhibiting Structural Simplicity and Ion Channel Activity. *Chem. - Eur. J.* **2009**, *15*, 10543−10553.

(20) (a) Gale, J. D.; Rohl, A. L. The general utility lattice program (GULP). *Mol. Simul.* **2003**, *29*, 291−341. (b) Mayo, S. L.; Olafson, B. D.; Goddard, W. A. DREIDING: a generic force field for molecular simulations. *J. Phys. Chem.* **1990**, *94*, 8897−8909. (c) Saha, T.; Dasari, S.; Tewari, D.; Prathap, A.; Sureshan, K. M.; Bera, A. K.; Mukherjee, A.; Talukdar, P. Hopping-Mediated Anion Transport through a Mannitol-Based Rosette Ion Channel. *J. Am. Chem. Soc.* **2014**, *136*, 14128−14135.

(21) (a) Chao, S.; Romuald, C.; Fournel-Marotte, K.; Clavel, C.; Coutrot, F. A Strategy Utilizing a Recyclable Macrocycle Transporter for the Efficient Synthesis of a Triazolium-Based [2] Rotaxane. *Angew. Chem., Int. Ed.* **2014**, *53*, 6914−6919. (b) Coutrot, F.; Busseron, E. A new glycorotaxane molecular machine based on an anilinium and a triazolium station. *Chem. - Eur. J.* **2008**, *14*, 4784−4787.

(22) (a) Vukotic, V. N.; Zhu, K. L.; Baggi, G.; Loeb, S. J. A pyridinium/anilinium [2] catenane that operates as an acid−base driven optical switch. *Angew. Chem., Int. Ed.* **2017**, *56*, 1−7. (b) Kovaricek, P.; Lehn, J. M. Merging constitutional and motional covalent dynamics in reversible imine formation and exchange processes. *J. Am. Chem. Soc.* **2012**, *134*, 9446−9455.

(23) Vukotic, V. N.; Zhu, K. L.; Baggi, G.; Leob, S. J. Optical Distinction Between ″Slow″ and ″Fast″ Translational Motion in Degenerate Molecular Shuttles. *Angew. Chem., Int. Ed.* **2017**, *56*, 1−7.

(24) (a) Chen, S.; Zhao, Y.; Bao, C.; Zhou, Y.; Wang, C.; Lin, Q.; Zhu, L. A well-defined unimolecular channel facilitates chloride transport. *Chem. Commun.* **2018**, *54*, 1249−1252. (b) Liu, T.; Bao, C.; Wang, H.; Lin, Y.; Jia, H.; Zhu, L. Light-controlled ion channels formed by amphiphilic small molecules regulate ion conduction via cis−trans photoisomerization. *Chem. Commun.* **2013**, *49*, 10311−10313.

(25) Matile, S.; Sakai, N. In *Analytical Methods in Supramolecular Chemistry*; Wiley-VCH Verlag GmbH & Co.: KGaA, 2007; p 391.

(26) Ren, C.; Zeng, F.; Shen, J.; Chen, F.; Roy, A.; Zhou, S.; Ren, H.; Zeng, H. Pore-Forming Monopeptides as Exceptionally Active Anion Channels. *J. Am. Chem. Soc.* **2018**, *140*, 8817−8826.

(27) Fyles, T. M.; Loock, D.; Zhou, X. A voltage-gated ion channel based on a bis-macrocyclic bolaamphiphile. *J. Am. Chem. Soc.* **1998**, *120*, 2997−3003.

(28) Jones, J. E.; Diemer, V.; Adam, C.; Raftery, J.; Ruscoe, R. E.; Sengel, J. T.; Wallace, M. I.; Bader, A.; Cockroft, S. L.; Clayden, J.; Webb, S. J. Length-dependent formation of transmembrane pores by helical α-aminoisobutyric acid foldamers. *J. Am. Chem. Soc.* **2016**, *138*, 688−695.

(29) Eisenman, G.; Horn, R. J. Membr. Biol. Ionic selectivity revisited: the role of kinetic and equilibrium processes in ion permeation through channels. *J. Membr. Biol.* **1983**, *76*, 197−225.

(30) Hu, X.-B.; Chen, Z.; Tang, G.; Hou, J.-L.; Li, Z.-T. Single-molecular artificial transmembrane water channels. *J. Am. Chem. Soc.* **2012**, *134*, 8384−8387.

(31) Chui, J. K.W.; Fyles, T. M. Ionic conductance of synthetic channels: analysis, lessons, and recommendations. *Chem. Soc. Rev.* **2012**, *41*, 148−175.

(32) Serreli, V.; Lee, C. F.; Kay, E. R.; Leigh, D. A. A molecular information ratchet. *Nature* **2007**, *445*, 523−527.

(33) (a) Murillo, O.; Watanabe, S.; Nakano, A.; Gokel, G. W. Synthetic models for transmembrane channels: structural variations that alter cation flux. *J. Am. Chem. Soc.* **1995**, *117*, 7665−7679. (b) Buste, D. C.; Hinton, J. F.; Millett, F. S.; Shungu, D. C. ^{23}Na-nuclear magnetic resonance investigation of gramicidin-induced ion transport through membranes under equilibrium conditions. *Biophys. J.* **1988**, *53*, 145−152.

DOI: 10.1021/jacs.8b09580
J. Am. Chem. Soc. 2018, 140, 17992−17998